Lithuanian Journal of Physics
Vol. **65**, No. 4, pp. 223–235 (2025)
ISSN 1648-8504 eISSN 2424-3647
DOI: https://doi.org/10.3952/physics.2025.65.4.5

CONTROL OF PROTON IRRADIATION-INDUCED DAMAGE IN LOW GAIN AVALANCHE DETECTORS BY HEAT TREATMENT TECHNIQUES

L. Deveikis, M. Biveinytė, T. Čeponis, E. Gaubas, V. Rumbauskas, and K. Žilinskas

Institute of Photonics and Nanotechnology, Vilnius University, Saulėtekio 3, 10257 Vilnius, Lithuania
Email: laimonas.deveikis@tmi.vu.lt

Received 21 October 2025; accepted 16 November 2025

Silicon-based particle sensors are widely employed in high-energy and nuclear physics experiments conducted at the European Organization for Nuclear Research (CERN). In recent years, silicon sensors with internal gain, known as low gain avalanche detectors (LGADs), have demonstrated an excellent performance in detecting high-energy particles owing to their good spatial and timing resolution. The sensor LGAD architecture has shown a great potential for the use in the upcoming High-Luminosity Large Hadron Collider (HL-LHC) upgrade, where semiconductor sensors will be exposed to extremely high radiation fluences. In this study, the impact of high-energy proton irradiation on the electrical performance of LGADs was investigated. The variations of critical parameters such as leakage current, effective doping concentration, carrier lifetime, spectral characteristics of radiation-induced defects, and charge collection, before and after thermal annealing at different temperatures, have been analysed using the *I*–*V*, *C*–*V*, microwave-probed photoconductivity (MW-PC), photoionization spectroscopy (PIS), and transient current (TCT) methods. It was demonstrated that the 24 GeV energy proton irradiation introduces defects, such as divacancy and trivacancy complexes, boron–oxygen and carbon–oxygen complexes, as well as divacancy–oxygen and divalent bistable defects, which act as current generation and carrier recombination centres. Annealing at temperatures of up to 400°C led to the transformation or passivation of those defects, partially restoring doping profiles and improving carrier lifetimes. These results highlight the potential of defect engineering to enhance the radiation tolerance of LGADs employed in high-energy physics applications.

Keywords: low-gain avalanche detectors, radiation-induced defects, recombination lifetime, spectroscopy of defects

1. Introduction

Precise particle tracking and timing are critical requirements for detectors in modern high-energy physics (HEP) experiments, operating at high luminosities and particle rates, such as those anticipated in the High-Luminosity Large Hadron Collider (HL-LHC) upgrade at CERN [1]. Silicon-based detectors have long been employed for particle tracking owing to their excellent charge collection properties, high granularity, and compatibility with established readout technologies. However, the extreme radiation environment, expected at the HL-LHC, with hadron fluences exceeding 10^{16} cm^{-2}, raises significant challenges to the longevity and performance of these sensors [2].

Low gain avalanche detectors (LGADs) comprise a class of silicon sensors that incorporate a thin, heavily doped gain layer, enabling internal charge multiplication through impact ionization. This design enables fabrication of thin detectors with enhanced time resolution [3]. As a result, LGADs achieve the timing resolution of 20–50 ps [4] and are considered as the leading candidates for the timing layers of next-generation 4D tracking systems. Nevertheless, the performance of LGADs degrades under a large fluence irradiation due to the introduction of radiation-induced defects that affect leakage current, effective doping concentration, and charge carrier lifetime. In particular, acceptor removal in the gain layer [5–7] and the formation of deep-level recombination

and generation centres are among the primary reasons limiting the radiation hardness of LGADs.

In this work, we present a purposeful study of LGADs irradiated with 24 GeV/c momentum relativistic protons at fluences of up to 10^{16} cm^{-2}. Radiation-induced damage and its evolution under isochronal annealing at a temperature range of 80–400°C have been characterized using a combination of electrical and spectroscopic techniques: current–voltage (I–V), capacitance–voltage (*C*–*V*), microwave-probed photoconductivity (MW-PC), photoionization spectroscopy (PIS), and transient current technique (TCT). The variations of the key parameters, such as leakage current, effective doping concentration, charge carrier lifetime, activation energies of defects and collected charge were examined. These results provide insights into the mechanisms of defect formation and annealing in the irradiated LGADs. This also highlights the potential of thermal treatments to partially restore sensor performance, thereby advancing the development of radiation-tolerant LGAD technologies for the next-generation HEP experiments.

2. Samples and experimental techniques

2.1. Samples

The studied samples were fabricated at the *Centro Nacional de Microelectrónica* (*CNM*) in the framework of CERN DRD3 collaboration. The devices were designed using the $n^{++}p^{+}\pi p^{++}$ low gain avalanche detector (LGAD) architecture. They were produced from a 50 μm thick float-zone silicon wafer grown on a 300 μm thick low-resistivity Czochralski wafer that served as mechanical support. The sensor structures consisted of a 300 μm p^{++} support wafer, a 50 μm active p-type layer, and a highly-doped 1 μm n^{++} cathode region. The dopant concentration in the n^{++} region was in an order of 10^{18}–10^{19} cm^{-3}. Additionally, the sensors had an implanted highly-doped p^{+} multiplication layer with a dopant concentration in an order of 10^{16} cm^{-3} to implement the internal gain. Each device had an active area of 1.3 × 1.3 mm^2, covered by aluminium surface metallization and surrounded by a guard ring. A square non-metalized window of 200 × 200 μm^2 area was formed within the cathode electrode for the optical excitation of carriers. A gold bump was deposited on the cathode Al layer to improve the electrical contact. An optical microscopy image and a schematic cross-sectional view of the device structure are shown in Fig. 1.

Proton irradiations of the investigated LGADs were carried out at CERN using 24 GeV/c relativistic protons, and fluences Φ ranging from 10^{12} to 10^{16} cm^{-2}. Following the initial electrical characterization, the samples underwent isochronal 30 min annealing at temperatures between 80 and 400°C. To prevent the oxidation of electrodes at higher temperatures, the annealing above 300°C was performed using the argon gas ambient atmosphere.

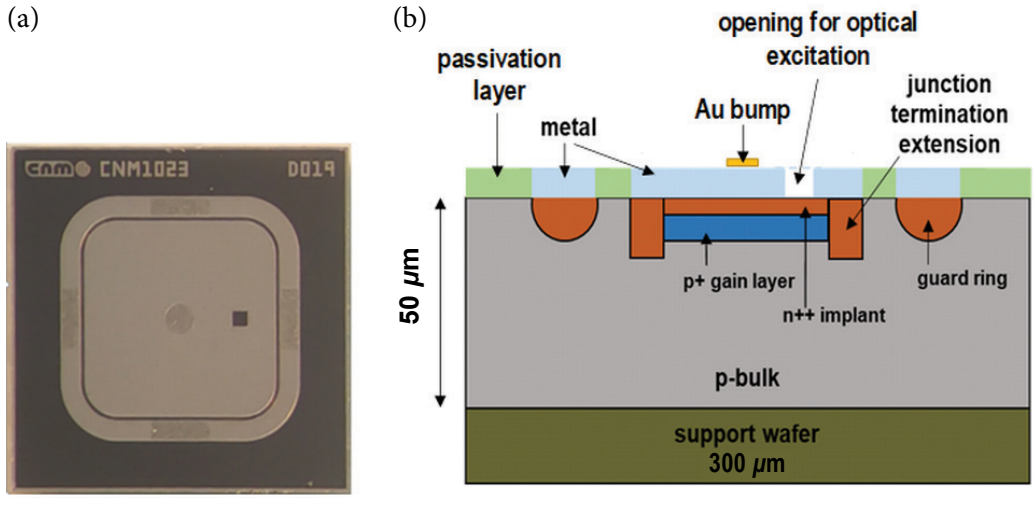

Fig. 1. An optical microscopy image (a) and a schematic cross-sectional view (b) of the LGAD structure.

2.2. Experimental techniques

Current–voltage (*I–V*) and capacitance–voltage (*C–V*) measurements were carried out using a Summit™ 11000B-AP probe station, integrated with a *Keysight* E4980A *LCR* meter and a *Keysight* B2912B source/measure unit (SMU).

The carrier recombination time variations were examined using the MW-PC transient technique [8], where the excess carriers have been photoexcited by 1062 nm wavelength pulsed (400 ps) illumination using a laser beam focused to ≤50 μm of the diameter and generated by an STA-01 YAG:Nd laser setup. The excited spot-area was probed with 22 GHz microwaves using a slit antenna and implementing LGAD depth-integrated lifetime measurements. There, the excess carrier decay transients were recorded using a 1 GHz oscilloscope TDS-5104. For the sensor characterization, the LGADs were oriented vertically with respect to the slit MW antenna, enabling both excitation and probing through the polished edge of the sensor. The MW response is proportional to the excess carrier concentration $n(t)$. For the as-irradiated samples, the MW-PC transients typically follow a single-exponential decay $n(t) = n(t = 0)\cdot\exp(-t/\tau_R)$, with τ_R representing the recombination lifetime.

Quasi-steady-state photoionization spectroscopy (PIS) was employed to extract the photoactivation energies of radiation-induced defects. There, the photocurrent was measured on the edge-illuminated device using an 800 W photometric lamp excitation which was spectrally dispersed by a DMR-4 double-prism monochromator. The samples were mounted in a liquid nitrogen cryostat, equipped with VIS–IR transparent windows, and the temperature was stabilized at 78 K. Measurements were conducted using a Keithley 2635B electrometer at the applied reverse bias of 20 V. The resulting PI spectra exhibited multiple spectral steps, each associated with a definite trap of photoactivation energy E_n. The PI signal depends on the incident photon energy $h\nu$ through the photon–electron interaction cross-section $\sigma(h\nu)$, which governs the shape and position of PI spectral steps. This dependence is well described by the Kopylov–Pikhtin [9] model

$$\sigma(h\nu) = M_{ik}^2 \int_0^\infty \frac{\mathrm{e}^{-(E+E_n-h\nu)^2/\Gamma^2}\sqrt{E}\,\mathrm{d}E}{h\nu(E+E_n)^2}. \qquad (1)$$

Here, Γ is the broadening parameter related to the Huang–Rhys factor, the Franck–Condon shift, and the vibrational mode energy. M_{ik} is the matrix element for the dipole transitions from an initial (i) trap level to the continuum (k) state.

Charge collection measurements were performed using a commercial system developed by *Particulars, Advanced Measurement Systems*. In this setup, non-equilibrium charge carriers were injected using 300 ps laser diode pulses at the 1064 nm wavelength. The excitation intensity was adjusted by varying the laser diode current, while the bias voltage was supplied by a *Keithley* 2410 SMU. Transient current signals were recorded using a 2.5 GHz *LeCroy* WR9254 oscilloscope. To minimize the noise, the samples were mounted on custom-designed printed circuit boards (PCB) enclosed in a copper-shielded chamber. This assembly was attached to a three-axis computer-controlled translation stage, enabling the precise positioning of the carrier injection through the non-metallized window within the sensor electrode. The measurements of the injected charge drift currents were performed at room temperature in the dark.

3. Experimental results

3.1. Characteristics obtained in as-irradiated LGADs

3.1.1. Electrical characteristics

The *I–V* characteristics (Fig. 2(a)) measurements performed in the 0–150 V reverse bias voltage (U_R) range reveal an increase in leakage current with rising proton fluence, indicating cumulative radiation damage in the detectors.

The step-like increase of current observed within the *I–V* curves is related to the full depletion of the active layer of LGADs, following after the depletion of the gain layer. A tendency of the shift of this current-change step towards lower voltages indicates a reduction in the effective doping concentration of the gain layer. At the highest fluence of 10^{16} cm^{-2}, the step-like current change is no longer visible, suggesting that the dopant concentration in the gain layer has decreased to a level comparable with that inherent for the underlying active region. This behaviour of current changes is consistent with radiation-induced acceptor removal effects [10].

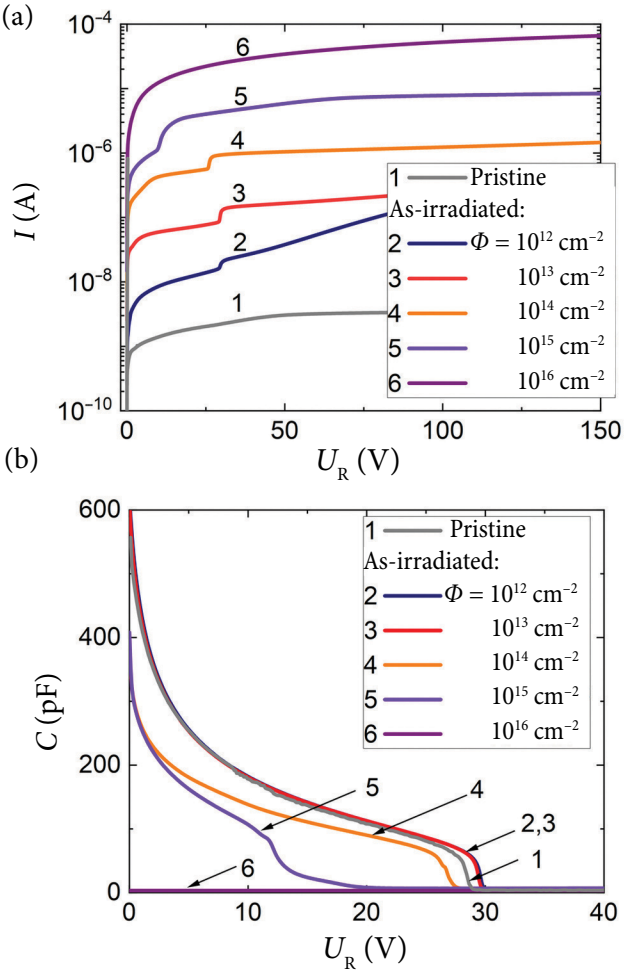

Fig. 2. *I–V* (a) and *C–V* (b) characteristics measured in LGADs irradiated with proton fluences in the 10^{12}–10^{16} cm^{-2} range and compared with the characteristics obtained for the non-irradiated (pristine) diode.

The *C–V* characteristics (Fig. 2(b)) corroborate the *I–V* results. Here, the barrier capacitance of a diode decreases after irradiations with fluences >10^{13} cm^{-2}, and the step-like drop of capacitance value, associated with the full depletion of the active region, shifts toward lower voltages under increase of fluence. This reduction in capacitance confirms a corresponding decrease in the effective dopant concentration in both the gain and the active layers. This capacitance reduction feature provides evidence of the radiation-induced removal of the acceptor-dopants and, thereby, the degradation of the gain layer.

3.1.2. Carrier recombination characteristics

The MW-PC transients measured in pristine and proton irradiated LGADs are illustrated in Figs. 3(a, b) for different proton fluence levels. In the non-irradiated and 10^{12} cm^{-2} proton fluence irradiated diodes, the transients exhibit a short initial decay fragment, associated with the surface

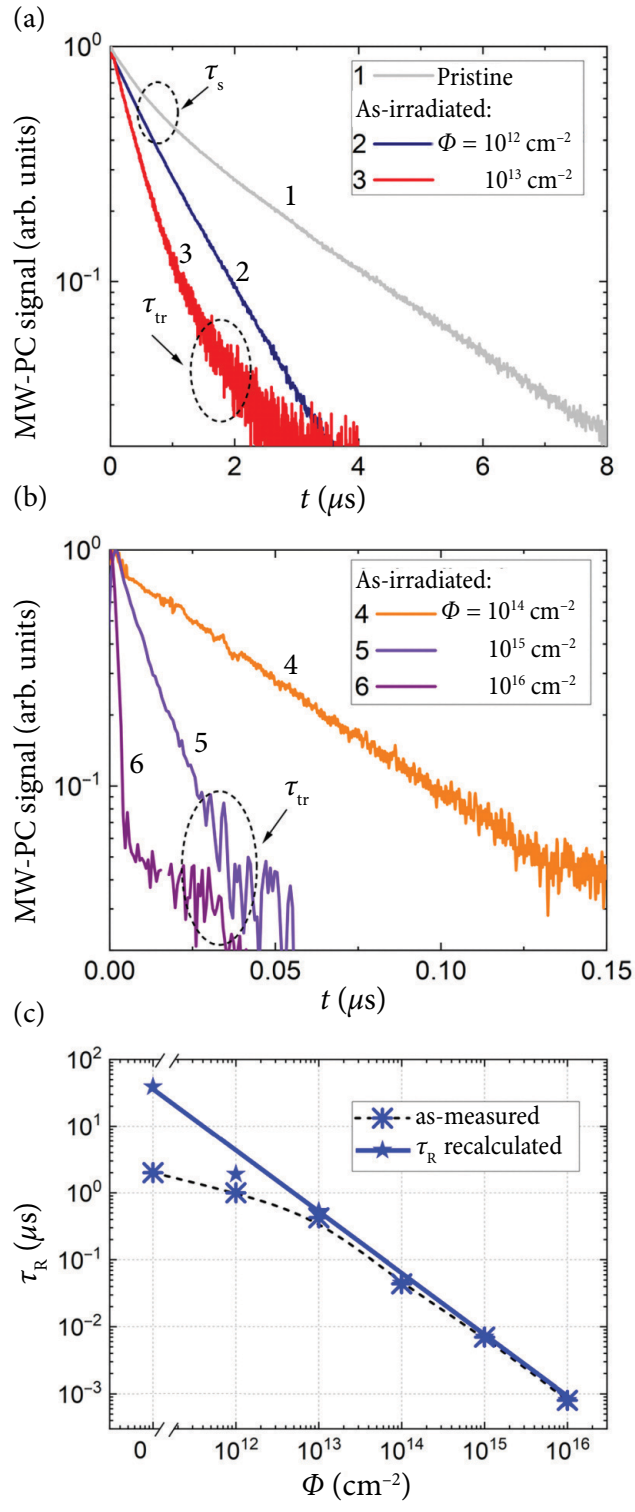

Fig. 3. MW-PC transients measured in pristine and proton irradiated LGAD samples with different fluences (a, b) and extracted carrier recombination lifetime values as a function of proton irradiation fluence (c).

recombination τ_s constituent, and the longer relaxation component attributed to the bulk recombination lifetime τ_R. At elevated fluences, the relaxation rate increases, indicating a reduction in the effective carrier recombination lifetime. This behaviour reflects the increasing density of radiation-induced recombination centres, which accelerates carrier recombination within the irradiated material. At sufficiently high fluences, the surface recombination component becomes negligible when $\tau_R << \tau_s$. Notably, in LGADs irradiated with fluences of 10^{13}, 10^{15} and 10^{16} cm^{-2}, an additional longer relaxation component emerges within the MW-PC transients. This long-tail decay constituent is attributed to the carrier trapping τ_{tr}, where multiple deep and shallow level species within the bandgap govern the excess carrier decay dynamics, as discussed in detail in Ref. [8]. The extracted bulk recombination lifetime values, recalculated by the subtracting impact of surface recombination, are summarized in Fig. 3(c) as a function of proton irradiation fluence. The τ_R is inversely proportional to the irradiation fluence and the estimated τ_R decreases from 40 μs in the pristine sample to <1 ns in the sample exposed to the highest fluence of 10^{16} cm^{-2} (Fig. 3(c)). This strong degradation in lifetime is attributed to the formation of radiation-induced defects acting as deep-level recombination centres within the silicon material and acting in parallel with the present trapping centres, which also determine the degradation of temporal characteristics of the LGADs.

3.1.3. Photoionization spectra

For the characterization of the dominant radiation-induced traps as well as those present within the pristine material, photoionization spectroscopy has been performed. The step-like photoionization spectra have been observed and simulated using the Kopylov–Pikhtin approach [9]. In the non-irradiated diode (Fig. 4(a)), two defect-related energy levels have been distinguished at E_1 = 0.99 eV and E_2 = 0.88 eV associated with a complex of divacancy and trivacancy (V_2 + V_3) E_1 [11] and the interstitial boron–interstitial oxygen (B_iO_i) complex E_2 [12], respectively. The presence of these defects within the non-irradiated material could be explained by the inevitable radiation damage introduced during the formation of gain layer by the implantation of boron atoms. With the enhancement of irradiation fluence, the amount of the observed defect species also increased.

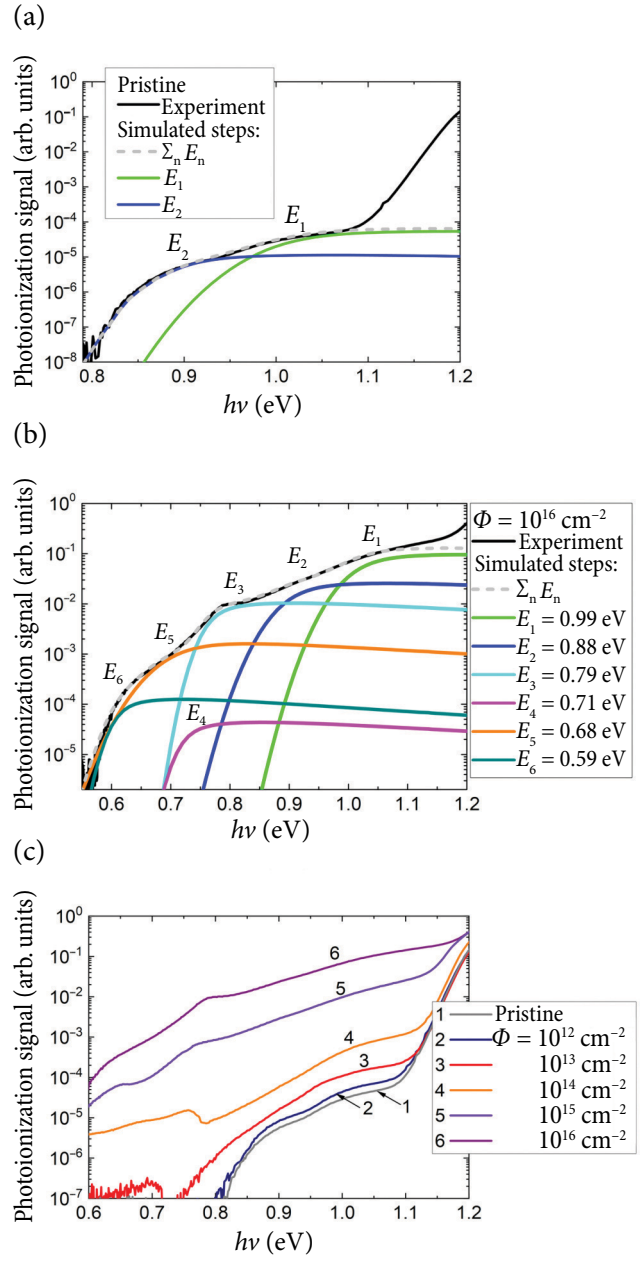

Fig. 4. PIS spectra obtained in pristine (a) and proton irradiated (b) with the fluence of Φ = 10^{16} cm^{-2} LGADs. Here, the solid black lines represent the recorded spectra, while the colour lines correspond to particular energy levels simulated using the Kopylov–Pikhtin approach. The dashed grey lines represent the sum of all resolved spectral steps. (c) The comparison of PIS spectra measured in LGADs irradiated with varying fluences in a range of Φ = 10^{12}–10^{16} cm^{-2}. Here, the spectra are normalized to the peak value of the spectral step ascribed to the band gap energy E_g.

Namely, in the spectrum of the LGAD exposed to the highest fluence of 10^{16} cm^{-2} (Fig. 4(b)), four additional radiation defect-related energy levels have been resolved at E_3 = 0.79 eV, E_4 = 0.71 eV, E_5 = 0.68 eV and E_6 = 0.59 eV. The energy levels resolved by photoionization spectroscopy have then been attributed to specific defect types by adjusting the obtained parameters to those reported in the literature. The defects identified using activation energy values of the resolved levels are listed in Table 1.

The increase in the photocurrent value observed in the photoionization spectra correlates with the rise in defect concentration, linked with the proton fluence. The energy level at E_2, attributed to the B_iO_i complex, plays a key role in the acceptor removal process [7]. This complex renders the boron atom electrically inactive by forming a chemically stable configuration with oxygen that is ubiquitous in float-zone silicon. Other identified defects include the interstitial carbon-interstitial oxygen (C_iO_i) complex [13] E_3, the divalent bistable defect (DBH) [14] E_4, the divacancy-oxygen (V_2O) complex [13, 15] E_5, and the silicon interstitial atom related I-centre complex [15] E_6. Notably, the identified defect types are consistent with those observed by deep-level transient spectroscopy (DLTS) and PIS in similar LGADs, fabricated by *Hamamatsu Photonics* [16].

3.2. Characteristics obtained in thermally annealed LGADs

3.2.1. Electrical characteristics in thermally annealed devices

Following the initial characterization, all samples were subjected to isochronal τ_{an} = 30 min annealing steps at temperatures T_{an} ranging from 80 to 400°C. The evolution of the *I–V* characteristics for the sample irradiated with a fluence of 10^{16} cm^{-2} is illustrated in Fig. 5(a), while the leakage current $I|_{UR\ =\ 150\ V}$) at an applied reverse bias of U_R = 150 V for all the examined irradiation fluences is summarized in Fig. 5(b). For LGADs irradiated with fluences ≥10^{14} cm^{-2}, the annealing caused a decrease in the leakage current, which was observed throughout the whole temperature range of thermal treatments, indicating either the decrease of the density of radiation-induced defects or transformations of radiation-induced generation centres turning them electrically inactive. In contrast, diodes irradiated with lower fluences (≤10^{13} cm^{-2}) exhibited an increase in the leakage current at higher annealing temperatures, likely due to the configuration transformations of the generation centres. These variations of the current characteristics reflect diversity in the dominant defect species and their concentrations, dependent on proton fluence [17, 18].

Table 1. Activation energy values, with respect to valence (E_v) and conduction (E_c) band energies, extracted from the photoionization spectra of non-irradiated and irradiated with proton fluences in a range of 10^{12}–10^{16} cm^{-2} LGAD samples, along with the corresponding defect types attributed to each identified level.

Φ, cm^{-2}	E_1, eV	E_2, eV	E_3, eV	E_4, eV	E_5, eV	E_6, eV
	Type of defect					
	$V_2 + V_3$ [11]	B_iO_i [12]	C_iO_i [13]	DBH [14]	V_2O [13,15]	I-centre [15]
0	0.99 E_v + 0.18	0.88 E_c–0.29	–	–	–	–
10^{12}	0.99 E_v + 0.18	0.88 E_c–0.29	–	–	–	–
10^{13}	0.99 E_v + 0.18	0.88 E_c–0.29	0.79 E_v + 0.38	–	–	–
10^{14}	0.99 E_v + 0.18	0.88 E_c–0.29	0.79 E_v + 0.38	–	–	–
10^{15}	0.99 E_v + 0.18	0.88 E_c–0.29	0.79 E_v + 0.38	0.71 E_v + 0.46	0.68 E_c–0.49	0.59 E_v + 0.57
10^{16}	0.99 E_v + 0.18	0.88 E_c–0.29	0.79 E_v + 0.38	0.71 E_v + 0.46	0.68 E_c–0.49	0.59 E_v + 0.57

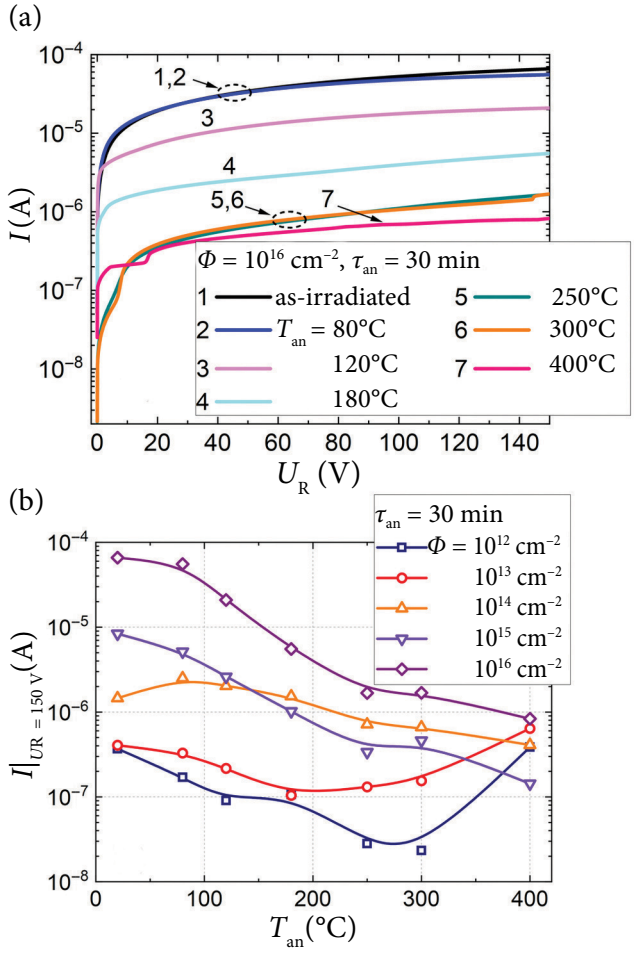

Fig. 5. *I–V* characteristics in an LGAD irradiated with a proton fluence of 10^{16} cm^{-2} before and after 30-minute isothermal annealing steps at various temperatures (a) and variations of leakage current values measured at U_R = 150 V as a function of annealing temperature for the diodes irradiated with fluences in a range of $\Phi = 10^{12} - 10^{16}$ cm^{-2} (b).

Complementarily, the *C–V* characteristics were examined before and after the annealing. These characteristics in the $1/C^2$ versus U_R representation have been analysed. The reverse voltage U_R range, corresponding to the depletion of the gain layer, was applied. There, the slope of the $1/C^2$ curve yields the effective doping concentration N_{eff} as [19])

$$N_{eff} = \frac{2}{e\varepsilon\varepsilon_0 S^2 \dfrac{d\left(1/C^2\right)}{dU_R}}. \quad (2)$$

Here, e is the elementary charge, ε and ε_0 are the permittivities of the material and vacuum, respectively, and S is the active area of the device.

The effective doping concentration in the gain layer of the pristine material LGAD was estimated to be 4×10^{16} cm^{-3}. In LGADs irradiated with fluences of 10^{12} to 10^{13} cm^{-2}, the slopes of the $1/C^2$ curves, and thus N_{eff}, remained almost invariable across the entire annealing temperature range, yielding a constant value of N_{eff} ~1.7×10^{16} cm^{-3}. In contrast, annealing-induced changes in the $1/C^2$ slopes were evident for the diodes irradiated with elevated fluences in the range from 10^{14} to 10^{16} cm^{-2} (Fig. 6). For the LGAD irradiated with 10^{14} cm^{-2} fluence, N_{eff} increased from 9.25×10^{15} cm^{-3} before annealing to 1.46×10^{16} cm^{-3} after annealing at T_{an} = 400°C. Similarly, for the 10^{15} cm^{-2} fluence irradiated sample, N_{eff} increased from 6×10^{15} to 1.15×10^{16} cm^{-3}. However, no clear trend of N_{eff} changes with annealing temperature was observed in the range of the highest fluence of 10^{16} cm^{-2} irradiated LGAD (Fig. 6(c)). This can be explained either by more complicated transformations of defects or thermal damage of the diode structure under heat treatment at the highest temperatures.

The extracted values on N_{eff} and their evolution with T_{an} for LGADs irradiated with proton fluences of 10^{14} and 10^{15} cm^{-2} are summarized in Fig. 6(d). The partial recovery of the effective doping concentrations to their initial values, obtained before irradiation, suggests that thermal annealing, using appropriate regimes, can restore, at least partially, the functional characteristics of LGADs.

3.2.2. Variations of recombination characteristics under thermal treatments

The MW-PC transients exhibit a clear trend of increasing carrier recombination time with rising annealing temperature. This effect becomes more pronounced at higher irradiation fluences. For the LGAD irradiated with the highest fluence of 10^{16} cm^{-2}, the recombination time increased from <1 ns before annealing to 44 ns after annealing at T_{an} = 400°C. In comparison, for the LGAD irradiated with the lower fluence of 10^{12} cm^{-2}, the lifetime increased from 0.74 μs before annealing to 3.7 μs after annealing when using the same heat-treatment temperature. These results indicate that thermal annealing effectively mitigates the impact of radiation-induced defects on functional characteristics of LGADs, with a more substantial role observed in heavily irradiated samples.

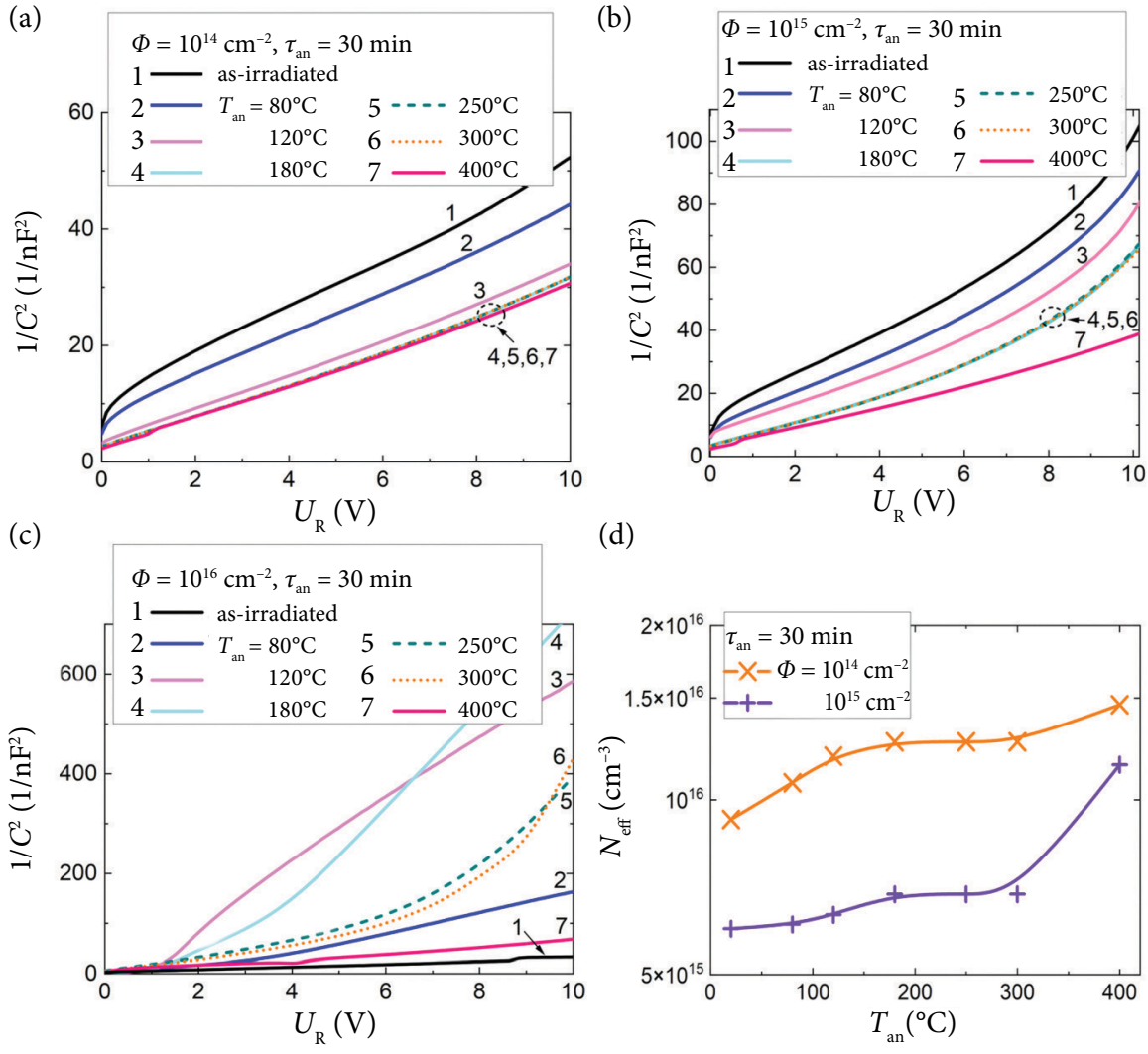

Fig. 6. Variations of barrier capacitance (as function $1/C^2$) characteristics measured in LGADs irradiated with proton fluences of 10^{14} (a), 10^{15} (b) and 10^{16} cm^{-2} (c) and isothermally annealed for τ_{an} = 30 min over the full annealing temperature T_{an} range from 80 to 400°C. (d) Variations of the effective dopant concentration N_{eff} within the gain layer of LGADs as a function of T_{an} for the samples irradiated with proton fluences of 10^{14} and 10^{15} cm^{-2}.

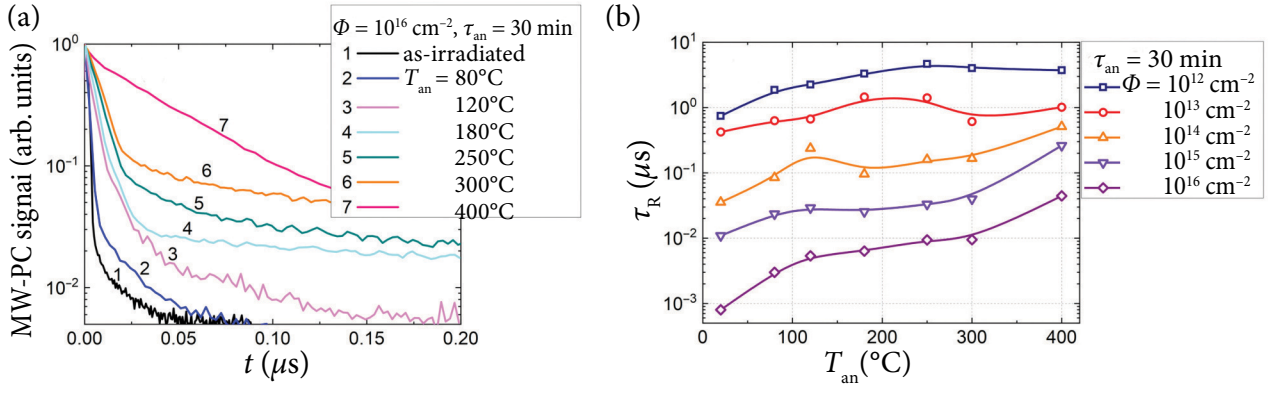

Fig. 7. (a) MW-PC transients recorded in the LGAD irradiated with a fluence of 10^{16} cm^{-2} and annealed at different temperatures in a range of 80–400°C. (b) Evolution of the carrier bulk recombination lifetime as a function of T_{an} for LGADs irradiated with different fluences.

Furthermore, in the diodes irradiated with elevated fluences (>10^{14} cm^{-2}), annealing implemented using the enhanced temperature of 400°C resulted in the emergence of a long-tail component within the MW-PC transients. This decay constituent hints at the appearance of carrier trapping [8] (Fig. 8). Together with the observed increase in bulk recombination lifetime, this implies that the concentration of deep recombination centres might be reduced in parallel with the formation of shallower carrier trapping centres upon high-temperature annealing.

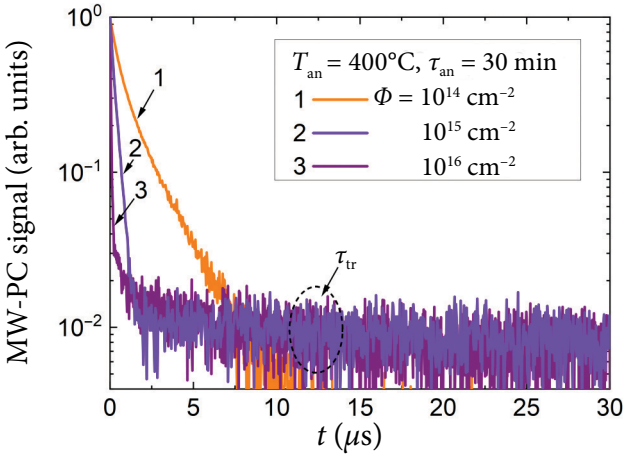

Fig. 8. A comparison of MW-PC transients recorded in LGADs irradiated with different proton fluences, ranging from 10^{14} to 10^{16} cm^{-2}, after isochronal annealing at 400°C. The long-tail decay component, attributed to carrier trapping, is clearly visible within the MW-PC transients recorded in LGADs irradiated with elevated fluences >10^{14} cm^{-2}.

3.2.3. Variations of photoionization spectra in heat-treated LGADs

In order to investigate the thermal annealing induced dissociation and transformation of radiation defects, photoionization spectra have been recorded in LGADs after each step of annealing. Significant changes within the PIS spectra (Fig. 9) were obtained after annealing at 400°C. The activation energies of defect levels extracted from the photoionization spectra, measured in the LGADs irradiated with proton fluences in a range of 10^{12}–10^{16} cm^{-2} and annealed at 400°C, along with identified radiation defect species, are summarized in Table 2. Specifically, two defect levels ascribed to the V_2O complex and

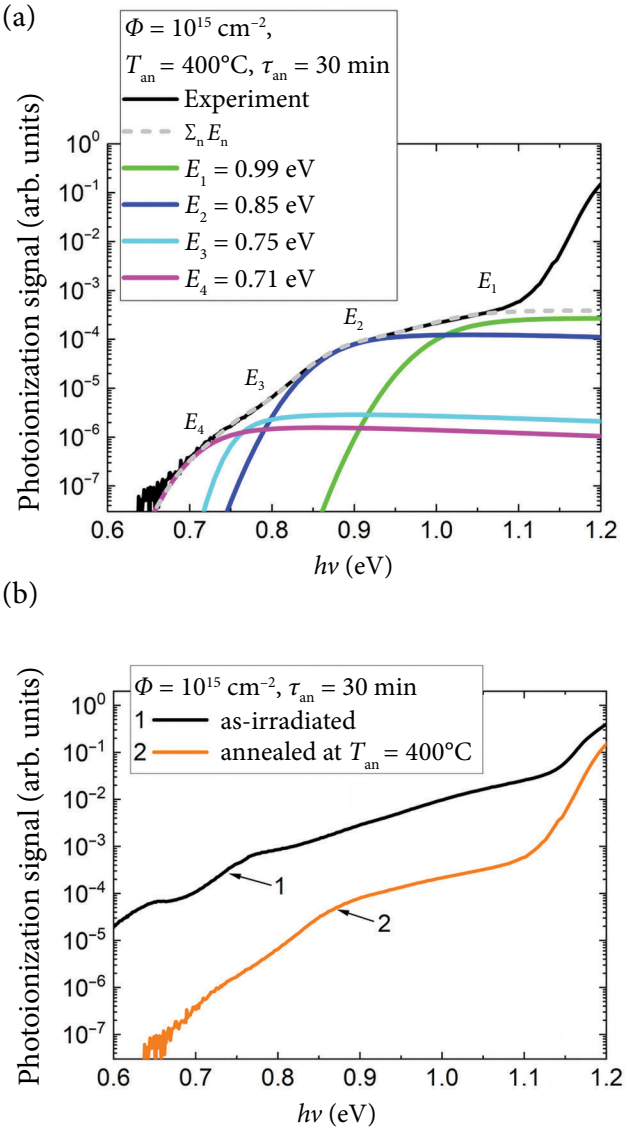

Fig. 9. (a) PIS spectrum with the simulated defect energy levels of the LGAD irradiated with the proton fluence of 10^{15} cm^{-2} and annealed at 400°C. (b) Comparison of PIS spectra for the same device before and after annealing at 400°C, highlighting the annealing induced changes of the spectrum structure.

I-centre, with activation energy values of E_5 = 0.68 eV and E_6 = 0.59 eV, were no longer present within the PI spectrum recorded in the LGAD annealed at 400°C, implying either their annihilation or transformation during the high-temperature treatment. Additionally, the activation energy values ascribed to centres E_2 as well as E_3 and associated with B_iO_i and C_iO_i complexes, respectively, shifted from 0.88 and 0.79 eV to 0.85 and 0.75 eV. These newly emerged centres can be attributed to the formation of a vacancy–oxygen–hydrogen (VOH) complex [20] and a vacancy-related centre (V_x) [21], as discussed in

Refs. [22–24]. The described transformations of the PIS spectrum after the thermal treatment also hint on the dissociation of previously identified B_iO_i and C_iO_i complexes. Furthermore, these defect transformations could also corroborate the observed restoring of effective dopant concentration in some of the annealed LGADs.

Table 2. Activation energy values of the defect levels extracted from the photoionization spectra recorded in the LGADs irradiated with proton fluences in a range of 10^{12}–10^{16} cm^{-2} and annealed at 400°C. The identified species of defects are also linked to these levels.

Φ, cm^{-2}	E_1, eV	E_2, eV	E_3, eV	E_4, eV
	Type of defect			
	$V_2 + V_3$ [11]	VOH [20]	V_x [21]	DBH [14]
10^{12}	0.99 E_v + 0.18	0.85 E_c–0.32	0.75 E_c–0.42	–
10^{13}	0.99 E_v + 0.18	0.85 E_c–0.32	0.75 E_c–0.42	–
10^{14}	0.99 E_v + 0.18	0.85 E_c–0.32	0.75 E_c–0.42	–
10^{15}	0.99 E_v + 0.18	0.85 E_c–0.32	0.75 E_c–0.42	0.71 E_v + 0.46
10^{16}	0.99 E_v + 0.18	0.85 E_c–0.32	0.75 E_c–0.42	0.71 E_v + 0.46

3.2.4. Annealing dependent charge collection properties in LGADs

Measurements of the collected charge Q by LGAD sensors were performed using the TCT technique by time-integrating the recorded current pulse. The measurements were performed using 1064 nm laser pulses for carrier injection with a pulse energy equivalent to approximately four minimum ionizing particles (MIPs). The measured collected charge in the as-irradiated and annealed at T_{an} = 400°C LGADs as a function of reverse voltage U_R is presented in Fig. 10. Here, the variations of the collected charge are shown by comparing the characteristics obtained for the non-irradiated reference and for LGADs irradiated with fluences of 10^{12} and 10^{13} cm^{-2}. The collected charge increases with the enhancement of U_R due to charge carrier multiplication within the gain layer of LGADs (Fig. 10(a)). Clear degradation in the charge collection with the increase of irradiation fluence has been observed

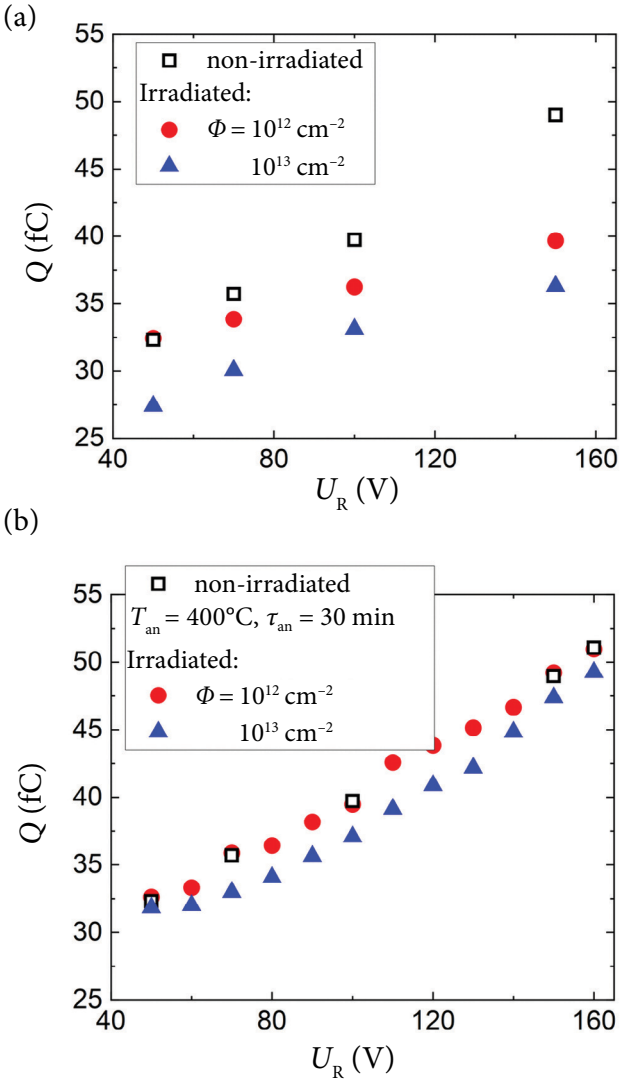

Fig. 10. Collected charge Q as a function of the applied reverse bias voltage U_R in the as-irradiated (a) and annealed at 400°C LGADs (b). The measured Q for a non-irradiated LGAD is also plotted as a reference.

before annealing, where the irradiated LGADs show a significantly less collected charge compared to that obtained in the non-irradiated ones, especially at elevated bias voltages. This reduction can be ascribed to the radiation-induced acceptor removal, which leads to the gain degradation of LGADs. This acceptor removal is usually followed by carrier recombination/trapping processes due to radiation-induced defects [16]. Fortunately, the collected charge value in the LGAD, irradiated with 10^{12} cm^{-2} fluence, recovers after thermal annealing at temperatures of 400°C to a value nearly identical to that of the non-irradiated device over the entire voltage range (Fig. 10(b)). The LGAD irradiated with 10^{13} cm^{-2} fluence also shows a substantial

improvement after the heat treatment, as the collected charge value approaches that of the reference device. The recovery of the collected charge is governed by the increase of the bulk recombination lifetime τ_R (Fig. 7(b)) after the heat treatment and recovery of N_{eff} (Fig. 6(d)). The latter enhancement of the N_{eff} after the heat treatment leads to the partial gain recovery in LGADs. This effect can, in parallel, be explained through the annealing-induced transformation or dissociation of defect complexes, such as B_iO_i.

4. Summary

The experimental results clearly demonstrate that high-energy proton irradiation introduces different electrically active defect centres in Si-based LGAD structures, significantly impacting their electrical performance. The observed increase in leakage current and the reduction in carrier lifetime with fluence can be attributed to the formation of deep-level generation and recombination centres such as divacancy and trivacancy ($V_{2/3}$), V_2O, B_iO_i, C_iO_i, DBH and I-centres, as identified from the PIS measurements. The strong correlation between the irradiation fluence and the emergence of new defect levels within the PIS spectra supports the progressive defect accumulation hypothesis, particularly for the fluences above 10^{14} cm^{-2}. Importantly, the disappearance of E_5 and E_6 levels and the shift of E_2 and E_3 spectral steps within the PIS spectra after annealing indicates that some of these defects are metastable and can be transformed or passivated by the thermal treatment. These transformations are likely related to the dissociation of B_iO_i and C_iO_i complexes and the subsequent formation of VOH and V_x-type centres.

The partial recovery of doping concentration within the gain layer of the LGADs irradiated with fluences of 10^{14}–10^{15} cm^{-2} suggests that a fraction of the boron dopants, rendered inactive due to acceptor removal reactions, can be reactivated by using the elevated annealing temperatures. This hypothesis is further supported by the post-annealing recovery of the collected charge, where in the LGAD, irradiated with 10^{12} cm^{-2} fluence, the collected charge completely recovers to values inherent for the non-irradiated reference device. The substantial improvement in the charge collection has also been obtained in the 10^{13} cm^{-2} fluence irradiated LGAD. These observations indicate that thermal annealing diminishes the concentration of radiation-induced defects. Heat treatments also efficiently restore the gain mechanism in moderately irradiated devices, thereby improving charge multiplication and overall detector response.

However, the inefficient recovery of the electrical LGAD characteristics in the 10^{16} cm^{-2} fluence irradiated devices indicates that either the majority of boron dopant atoms are persistently deactivated by the formation of defect complexes or defect clustering leads to irreversible structural changes, beyond a certain damage threshold. The emergence of the long-tail carrier trapping constituent within the MW-PC transients, in the heavily irradiated and annealed samples, is consistent with the presence of shallow traps formed during annealing. This implies that the concentration of deep recombination centres might be reduced in parallel with the formation of shallower carrier trapping centres upon high-temperature annealing, through the transformation of carrier recombination and trapping centres to those characterized by rather shallow states.

These findings underline the importance of tailoring post-irradiation annealing methods to balance defect passivation and dopant reactivation without triggering additional degradation mechanisms. Moreover, this study highlights the potential benefit of impurity engineering (e.g. carbon enrichment or hydrogenation) to control defect formation pathways and enhance the radiation tolerance of LGADs.

Acknowledgements

This research has been carried out in the framework of the agreement of Vilnius University with the Lithuanian Research Council No. VS-13. Giulio Pellegrini is acknowledged for providing the samples for investigation. The sample irradiations were performed in the framework of the European Union's Horizon Europe Research and Innovation Programme under Grant Agreement No. 101057511.

References

[1] G. Arduini, J. Barranco, A. Bertarelli, N. Biancacci, R. Bruce, O Bruning, X. Buffat, Y. Cai, L.R. Carver, and S. Fartoukh, High Luminosity

LHC: challenges and plans, JINST **11**, C12081 (2016).

[2] M. Moll, Displacement damage in silicon detectors for high energy physics, IEEE Trans. Nucl. Sci. **65**, 1561–1582 (2018).

[3] K. Onaru, K. Hara, D. Harada, S. Wada, K. Nakamura, and Y. Unno, Study of time resolution of low-gain avalanche detectors, Nucl. Instrum. Methods Phys. Res. A **985**, 164664 (2021).

[4] E. Currás, M. Fernández, and M. Moll, Gain reduction mechanism observed in Low Gain Avalanche Diodes, Nucl. Instrum. Methods Phys. Res. A **1031**, 166530 (2022).

[5] M. Moll, Acceptor removal – Displacement damage effects involving the shallow acceptor doping of p-type silicon devices, in: *Proceedings of the 28th International Workshop on Vertex Detectors (Vertex2019) – Radiation Effects* (SISSA, Trieste, 2020).

[6] R. Wunstorf , W.M. Bugg, J. Walter, F.W. Garber, and D. Larson, Investigations of donor and acceptor removal and long term annealing in silicon with different boron/phosphorus ratios, Nucl. Instrum. Methods Phys. Res. A **377**, 228–233 (1996).

[7] C. Besleaga, A. Kuncser, A. Nitescu, G. Kramberger, M. Moll, and I. Pintilie, Bistability of the B_iO_i complex and its implications on evaluating the acceptor removal process in p-type silicon, Nucl. Instrum. Methods Phys. Res. A **1017**, 165809 (2021).

[8] E. Gaubas, E. Simoen, and J. Vanhellemont, Review – Carrier lifetime spectroscopy for defect characterisation in semiconductor materials and devices, ECS J. Solid State Sci. Technol. **5**, P3108 (2016).

[9] A.A. Kopylov and A.N. Pikhtin, Influence of temperature on spectra of optical absorption by deep levels in semiconductors, Sov. Phys. Solid State **16**, 1200 (1975).

[10] C. Liao, E. Fretwurst, E. Garutti, J. Schwandt, M. Moll, and A. Himmerlich, The boron-oxygen (B_iO_i) defect complex induced by irradiation with 23 GeV protons in p-type epitaxial silicon diodes, IEEE Trans. Nucl. Sci. **69**(3), 576–586 (2022).

[11] S.D. Brotherton, G.J. Parker, and A Gill, Photoionization cross section of electron irradiation induced levels in silicon, J. Appl. Phys. **54**, 5112–5116 (1983).

[12] L.I. Khirunenko, M.G. Sosnin, A.V. Duvanskii, N.V. Abrosimov, and H. Riemann, Electronic absorption of interstitial boron-related defects in silicon, Phys. Status Solidi A **214**, 1700245 (2017).

[13] B.C. MacEvoy, G. Hall, and K. Gill, Defect evolution in irradiated silicon detector material, Nucl. Instrum. Methods Phys. Res. A **374**, 12–26 (1996).

[14] L.F. Makarenko, S.B. Lastovski, H.S. Yakushevich, E. Gaubas, J. Pavlov, V.V. Kozlovski, M. Moll, and I. Pintilie, Formation of a bistable interstitial complex in irradiated p-type silicon, Phys. Status Solidi A **216**, 1900354 (2019).

[15] E. Gaubas, A. Uleckas, and J. Vaitkus, Spectroscopy of neutron irradiation induced deep levels in silicon by microwave probed photoconductivity transients, Nucl. Instrum. Methods Phys. Res. A **607**, 92–94 (2009).

[16] T. Ceponis, M. Biveinyte, L. Deveikis, E. Gaubas, J. Pavlov, V. Rumbauskas, V. Tamosiunas, and K. Zilinskas, Characteristics of gain degradation in proton irradiated Low Gain Avalanche Detectors, JINST **20**, C08029 (2025).

[17] S. Lazanu and I. Lazanu, Correlation between radiation processes in silicon and long-time degradation of detectors for high-energy physics experiments, Nucl. Instrum. Methods Phys. Res. A **580**, 46–49 (2007).

[18] A. Himmerlich, N. Castello-Mor, E.C. Rivera, Y. Gurimskaya, V. Maulerova-Subert, M. Moll, I. Pintilie, E. Fretwurst, C. Liao, and J. Schwandt, Defect characterization studies on irradiated boron-doped silicon pad diodes and Low Gain Avalanche Detectors, Nucl. Instrum. Methods Phys. Res. A **1048**, 167977 (2023).

[19] D.K. Schroder, *Semiconductor Material and Device Characterisation* (John Wiley & Sons, Hoboken, New Jersey, 2006).

[20] I.L. Kolevatov, P.M. Weiser, E.V. Monakhov, and B.G. Svensson, Interaction between hydrogen and vacancy defects in crystalline silicon, Phys. Status Solidi A **216**, 1800670 (2019).

[21] V.V. Lukjanitsa, Energy levels of vacancies and interstitial atoms in the band gap of silicon, Semiconductors **37**, 404–413 (2003).

[22] J.H. Bleka, H. Malmbekk, E.V. Monakhov, and B.G. Svensson, Annealing dynamics of irradiation-induced defects in high-purity silicon in the presence of hydrogen, Phys. Rev. B **85**, 085210 (2012).

[23] M. Mikelsen, J.H. Bleka, J.S. Christensen, E.V. Monakhov, and B.G. Svensson, Annealing of the divacancy-oxygen and vacancy-oxygen complexes in silicon, Phys. Rev. B **75**, 155202 (2007).

[24] I.L. Kolevatov, B.G. Svensson, and E.V. Monakhov, Correlated annealing and formation of vacancy-hydrogen related complexes in silicon, J. Phys. Condens. Matter **31**, 235703 (2019).

PROTONAIS INDUKUOTOS RADIACINĖS PAŽAIDOS SENSORIUOSE SU VIDINIU STIPRINIMU VALDYMAS TAIKANT TERMINIO APDOROJIMO METODUS

L. Deveikis, M. Biveinytė, T. Čeponis, E. Gaubas, V. Rumbauskas, K. Žilinskas

Vilniaus universiteto Fizikos fakulteto Fotonikos ir nanotechnologijų institutas, Vilnius, Lietuva

Santrauka

Silicio pagrindu sukurti dalelių jutikliai plačiai naudojami aukštųjų energijų ir branduolinės fizikos eksperimentuose, vykdomuose CERN. Silicio jutikliai su vidiniu stiprinimu (vadinamieji *Low Gain Avalanche Detectors*, LGADs) pasižymi minėtuose eksperimentuose būtina erdvine ir laikine skyra ir laikomi vienu perspektyviausių technologinių sprendimų planuojamam didelio šviesingumo Didžiojo hadronų priešinių pluoštų greitintuvo (*High-Luminosity Large Hadron Collider*, HL-LHC) atnaujinimui, po kurio jutikliai turės atlaikyti ypač dideles spinduliuotės dozes.

Šiame darbe ištirta didelės energijos (24 GeV) reliatyvistinių protonų spinduliuotės įtaka silicio jutiklių su vidiniu stiprinimu elektrinėms charakteristikoms. Pasitelkus voltamperinių ir voltfaradinių charakteristikų matavimus, mikrobangomis zonduojamo fotolaidumo kinetikų analizę, fotojonizacijos spektroskopiją bei indukuoto krūvio dreifo srovių kinetikų matavimus, buvo ištirti nuotėkio srovės, efektinės legirantų koncentracijos, krūvininkų gyvavimo trukmės, radiacinių defektų spektrinių charakteristikų ir krūvio surinkimo efektyvumo pokyčiai jutikliuose su vidiniu stiprinimu prieš ir po terminių iškaitinimų įvairiose temperatūrose.

Buvo atskleista, kad protonų spinduliuotė sukelia defektų formavimąsi, tokių kaip divakansijų ir trivakansijų kompleksai, boro–deguonies, anglies–deguonies, divakansijos–deguonies kompleksai bei bistabilūs centrai. Šie defektai veikia kaip generaciniai arba rekombinaciniai centrai, nulemiantys jutiklių funkcinių charakteristikų kaitą. Parodyta, kad bandinių iškaitinimas iki 400 °C nulemia radiacinių defektų transformacijas ar dalies jų pasyvaciją, taip pat iš dalies atkuria legirantų koncentracijų pasiskirstymo profilius ir krūvininkų rekombinacijos trukmę. Aptarti rezultatai patvirtina defektų inžinerijos svarbą, siekiant padidinti jutiklių su vidiniu stiprinimu radiacinį atsparumą ir siekiant taikyti juos ateities aukštųjų energijų fizikos eksperimentuose.